Tetrahedron Vol. 49, No. 12, pp. 2361-2372, 1993
Printed in Great Britain

0040-4020/93 $6.00+.00

SELF-ASSOCIATION OF DIPYRRINONES OBSERVED BY 2D-NOE NMR AND DIMERIZATION CONSTANTS CALCULATED FROM ^{1}H-NMR CHEMICAL SHIFTS

Daniel F. Nogales,[a] Jin-Shi Ma[b] and David A. Lightner[a*]

[a]Department of Chemistry, University of Nevada, Reno, NV 89557-0020
and [b]The Institute of Photographic Chemistry, Academia Sinica, Beijing, China

(*Received in USA* 23 *November* 1992)

Abstract: *Methyl xanthobilirubinate (1) and methyl neoxanthobilirubinate (2) self associate, as seen by 2D-NOE NMR, to form hydrogen-bonded dimers in $CDCl_3$. Association constants $K_A \simeq 25{,}000$ (1) and 12,000 M^{-1} (2) at 22°C are derived from analysis of concentration-dependent N-H chemical shifts.*

(4Z,15Z)-Bilirubin-IXα, the yellow pigment of jaundice[1,2] is a dicarboxylic acid composed of two dipyrrinones conjoined by a -CH_2- group at C(10). Rotating the dipyrrinones about the -CH_2- group brings their lactam and pyrrole N-H groups into sufficiently close proximity to the propionic CO_2H groups for conformation-stabilizing hydrogen bonding. In solvents, such as $(CH_3)_2SO$, which act as strong hydrogen bond acceptors, solvent molecules bind competitively to the N-H groups, displacing the CO_2H groups from direct intramolecular hydrogen bonding. When the propionic acid groups are esterified or relocated away from the center of the molecule, or replaced by alkyls, intramolecular hydrogen bonding is also considerably weakened, and in non-hydrogen bonding solvents the dipyrrinone components tend to hydrogen bond intermolecularly,[3,4] The emerging picture for bilirubin and its derivatives and analogs is thus one where dipyrrinone hydrogen bonding, either intramolecular or intermolecular or with solvent, plays a major role in determining pigment shape and state of aggregation, as well as solution and spectroscopic properties.[4-6]

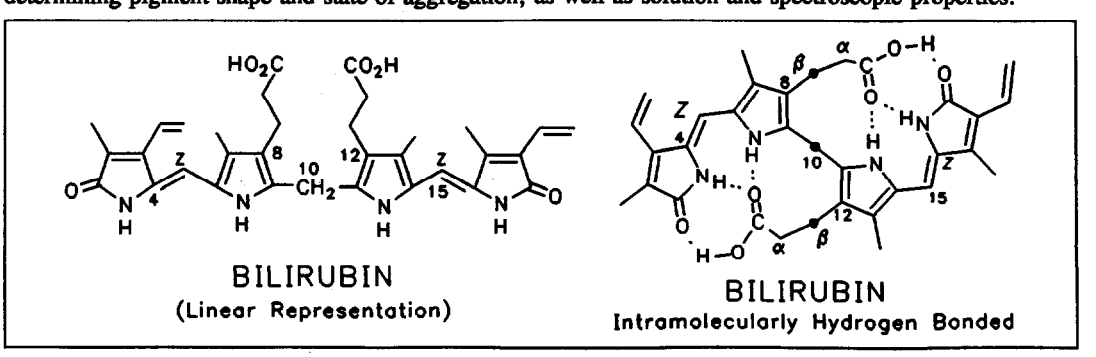

Dipyrrinone models equivalent to one-half of bilirubin are known to participate in hydrogen bonding: intermolecularly, in non-polar solvents such as chloroform; to solvent, in dimethylsulfoxide (Figure 1).[3,4,7,8]

Such hydrogen bonding has been detected by and analyzed from N-*H* chemical shifts in the ^{1}H-NMR.[4,5] The intermolecular hydrogen bonding is extensive, incorporating amide-amide hydrogen bonds between the lactam groups as well as those between pyrrole N-H and lactam carbonyl.[7-9] This unique network of four hydrogen bonds is apparently the major contributor to the large self-association constant ($K_A \simeq 1700\ M^{-1}$ at 37°C in $CHCl_3$) determined by vapor phase osmometry, because K_A is reduced by a factor of $\sim 10^3$ in dipyrrinones where only the lactam amide-amide hydrogen bonding is possible (as in dipyrrinones with the pyrrole nitrogen methylated).[3,10] In view of the importance of hydrogen bonding in dipyrrinones and bilirubin analogs, we present (i) our results on the detection of self-association in xanthobilirubic acid methyl ester (**1**) and neoxanthobilirubic acid methyl ester (**2**) (Figure 2) by NOE NMR measurements, and (ii) an NMR method for determining the self-dimerization association constants (K_A).

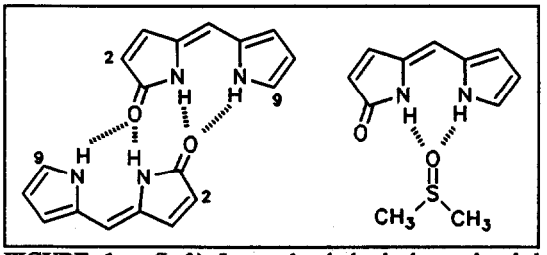

FIGURE 1. (Left) Intermolecularly hydrogen-bonded dipyrrinone dimer. (Right) Dipyrrinone hydrogen-bonded to dimethylsulfoxide.

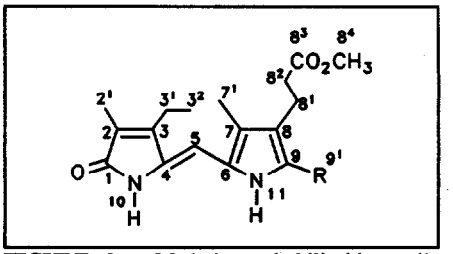

FIGURE 2. Methyl xanthobilirubinate (**1**, R=CH_3); methyl neoxanthobilirubinate (**2**, R=H).

RESULTS AND DISCUSSION

2-D NOE Correlations. The 2D homonuclear NOE spectra of $CDCl_3$ solutions of **1** and **2** are shown in Figures 3 and 4. The strong NOE's seen between the pyrrole and lactam N-H's near $\delta \sim 10.4$ and 11.3, respectively, and between the hydrogen at C(5) ($\delta \sim 6.2$) and the neighboring hydrogens at C(3^1) ($\delta \sim 2.6$) and C(7^1) ($\delta \sim 2.2$) are consistent with the pigment adopting a *Z*-configuration double bond at C(4) and with the pyrrole and lactam NH groups oriented in a *syn* periplanar or clinal conformation, as expected from earlier work.[3,4,9] Surprisingly perhaps, yet another NOE can be seen, a moderate NOE between the C(2) ($\delta \simeq 1.98$) and C(9) ($\delta \simeq 2.4$) methyl groups of **1** (2% NOE) and between the C(2) methyl ($\delta \simeq 1.98$) and C(9) hydrogen ($\delta \simeq 6.8$) of **2** (0.5% NOE). The large distances between these groups in **1** and in **2** preclude an *intra*molecular mechanism for the NOE, which can best be explained as emanating from an *inter*molecular mechanism where the relevant CH_3 group and other hydrogens are brought into close spatial proximity through a dimeric structure (Figure 4) proposed in previous work on dipyrrinone ^{1}H-NMR chemical shifts[3,4,8] and supported by vapor phase osmometry.[3,10] The intermolecular NOE vanishes in $(CD_3)_2SO$, a solvent which is known to disrupt dipyrrinone dimers, and is replaced by NOEs between the pyrrole and lactam N-*H*s and the small, residual methyl C-*H*'s of incompletely deuterated $(CD_3)_2SO$ solvent; however, the NOEs of intramolecular origin persist. The overall picture is consistent with the two cases formulated earlier: in non-hydrogen bonding solvents, dipyrrinones prefer to associate as hydrogen-bonded dimers; in dimethylsulfoxide, dipyrrinones exist as monomers that are hydrogen-bonded to solvent.[3,4,7-10] The presently reported intermolecular NOE measurements thus provide the first *direct* experimental observation of both cases.

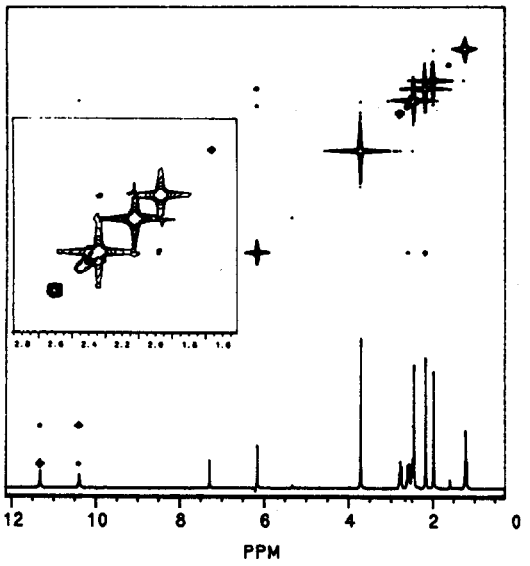

FIGURE 3. 2D-NOE plots for **1** in $CDCl_3$ at 21°C. Concentrations were 2.6 x 10^{-2} *M*.

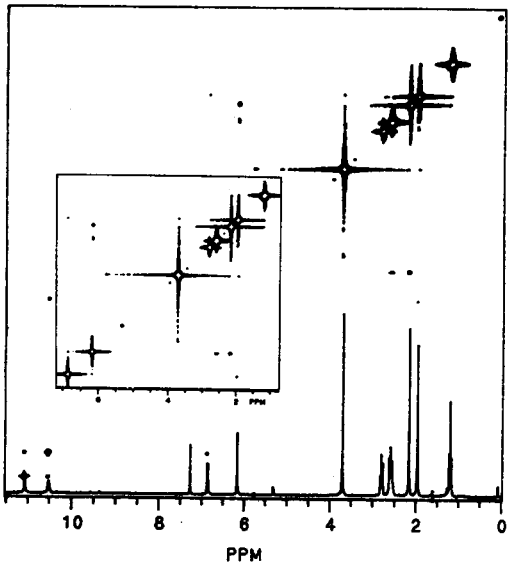

FIGURE 4. 2D-NOE plots for **2** in $CDCl_3$ at 21°C. Concentrations were 5.2 x 10^{-2} *M*.

Computing K_A. Dipyrrinone self-association in non-polar solvents has been assessed qualitatively by examining the N-*H* chemical shifts[4,8] and quantitatively through vapor phase osmometry to determine the average molecular weight and K_A.[3,10] The sensitivity of the N-*H* chemical shifts (δ_{obs}, Table 1) to hydrogen bonding from self-dimerization provides an alternative way to determine K_A. Either the lactam N-*H* or the pyrrole N-*H* signals may be used, but we found the latter to be more reliable because they are sharper, and thus δ_{obs} can be measured with more accuracy and less difficulty at the lowest sample concentrations.[11]

For the equilibrium $2M \rightleftarrows D$, the self-association, K_A, constant is described by:

$$K_A = \frac{[D]}{[M]^2} , \tag{1}$$

where the sum of monomer (M) and dimer (D) species is the initial concentration, $[M]_0$

$$[M]_0 = [M] + 2[D] . \tag{2}$$

The observed N-*H* chemical shift, δ_{obs}, is defined as (3) or (4)

$$\delta_{obs} = \delta_M + (\delta_D - \delta_M) \cdot \frac{2[D]}{[M]_0} \tag{3}$$

$$\delta_{obs} = \delta_M + (\delta_D - \delta_M) \cdot (1 - \frac{[M]}{[M]_0}) , \quad (4)$$

where δ_M and δ_D are the chemical shifts of the monomer and dimer, respectively, and $2[D]/[M]_0$ or $(1 - [M]/[M]_0)$ is the mole fraction of dimer. Expressing equations (3) and (4) in terms of [D] and [M], respectively, then substituting into equation (1) gives an expression for K_A in terms of $[M]_0$, δ_{obs}, δ_M and δ_D — as seen in equation (5) or its logarithmic expression (6):

$$K_A = \frac{(\delta_D - \delta_M)(\delta_{obs} - \delta_M)}{2\,(\delta_D - \delta_{obs})^2\,[M]_0} \quad (5)$$

$$\log\frac{2}{(\delta_D - \delta_M)} + \log K_A + \log [M]_0 = \log(\delta_{obs} - \delta_M) - 2\log(\delta_D - \delta_{obs}) \quad (6)$$

A plot of the right side of equation (6) *vs* log $[M]_0$ should give a straight line with intercept equal to log K_A + log 2 - log $(\delta_D - \delta_M)$.

Thus, in order to compute K_A, one must know δ_M and δ_D with good accuracy. When K_A is large, it is generally easier to extrapolate to an accurate value of δ_D than to δ_M because for the latter, the NMR measurement must be carried out at very high dilution, where instrument sensitivity can be the limiting factor. This is illustrated by the data of Table 1 and in Figure 5, where the chemical shifts of the pyrrole N-*H* (δ_{obs}) are plotted as a function of sample concentration ($[M]_0$) in $CDCl_3$ and $(CDCl_2)_2$ solvents (in which the pigments have the same behavior). At the highest concentrations of dipyrrinone, δ_{obs} reaches a plateau near $\delta \simeq 10.4$ and $\delta \simeq 10.5$ for the pyrrole N-*H* of **1** and **2**, respectively. At these concentrations the pigment is essentially completely dimerized. Similarly, for the lactam N-*H*, δ_{obs} reaches a plateau near $\delta \simeq 11.3$ and $\delta \simeq 11.1$ for **1** and **2**, respectively. In each case, the plateau value of δ_{obs} approaches δ_D, the N-*H* chemical shift for the pure dimer, D, and as the dipyrrinone concentrations drop, δ_{obs} approaches δ_M, the N-*H* chemical shift of the pure monomer, M. Clearly (see Figure 5), extrapolating δ_{obs} to δ_M in the limit $[M]_0 \to 0$ is more difficult than extrapolating to δ_{obs} to δ_D in the high concentration limit.

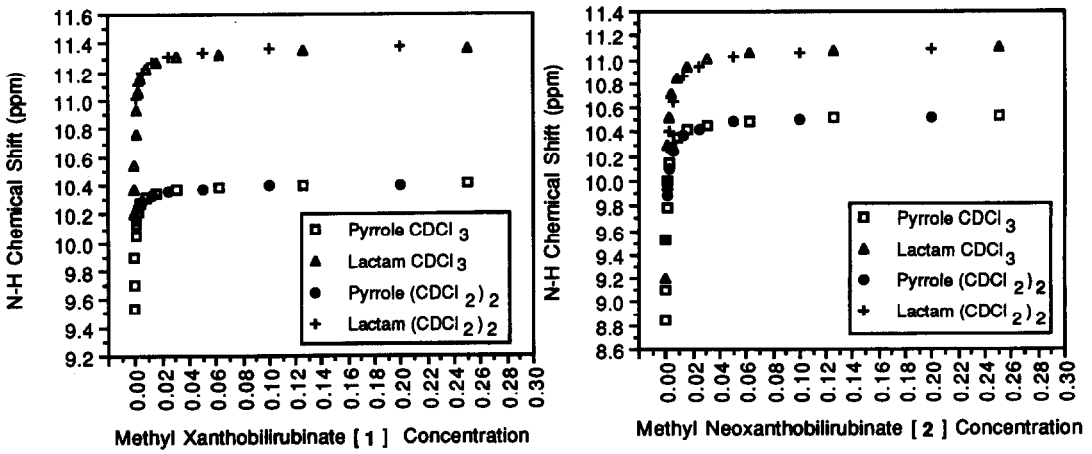

FIGURE 5. Plots of pyrrole and lactam N-*H* chemical shifts in $CDCl_3$ and $(CDCl_2)_2$ at 22°C *vs* dipyrrinone concentration for [left] methyl xanthobilirubinate (**1**) and [right] methyl neoxanthobilirubinate (**2**).

TABLE 1. Influence of Methyl Xanthobilirubinate (1) and Methyl Neoxanthobilirubinate (2) Concentration on Pyrrole and Lactam N-*H* Chemical Shifts (δ_{obs}) in $CDCl_3$ at 22°C.[a]

Dipyrrinone Conc. (M)	Methyl Xanthobilirubinate (1)		Methyl Neoxanthobilirubinate (2)	
	Lactam N-*H*	Pyrrole N-*H*	Lactam N-*H*	Pyrrole N-*H*
0.250	11.357	10.410	11.100	10.531
0.125	11.344	10.401	11.082	10.517
6.25×10^{-2}	11.327	10.390	11.050	10.494
3.125×10^{-2}	11.301	10.373	11.004	10.462
1.563×10^{-2}	11.266	10.350	10.938	10.418
7.812×10^{-3}	11.219	10.320	10.842	10.356
3.906×10^{-3}	11.152	10.277	10.711	10.271
1.953×10^{-3}	11.061	10.218	10.525	10.151
9.766×10^{-4}	10.933	10.136	10.291	9.997
4.883×10^{-4}	10.765	10.048	9.970	9.783
2.441×10^{-4}	10.542[b]	9.891[b]	9.532[b]	9.532
1.808×10^{-4}	10.371	9.700	9.200[d]	9.100[d]
9.039×10^{-5}	10.200[c]	9.535[c]	[c,e]	8.843[c,e]

[a] N-*H* chemical shifts in δ ppm downfield from $(CH_3)_4Si$ at 300 and 500 MHz. [b] Limits of sensitivity at 300 MHz. [c] Limits of sensitivity at 500 MHz. [d] 1.680×10^{-4} *M* pigment. [e] 8.402×10^{-5} *M* pigment.

Extrapolation to δ_D is achieved as follows. Rewriting equation (2) to solve for [D] then substituting for [D] in equation (1) and solving for [M] in the resulting quadratic equation gives the expression:

$$[M] = \frac{(1 + 8K_A [M]_0)^{1/2} - 1}{4K_A} . \tag{7}$$

Simplifying equation (4) gives:

$$\delta_{obs} = \delta_D - (\delta_D - \delta_M) \cdot \frac{[M]}{[M]_0} . \tag{8}$$

The expression for [M] in equation (7) is substituted for [M] in equation (8) to provide equation (9), an expression for δ_{obs} in terms of δ_D, δ_M, K_A and $[M]_0$.

$$\delta_{obs} = \delta_D - (\delta_D - \delta_M) \cdot \frac{(1 + 8K_A [M]_0)^{1/2} - 1}{4 K_A [M]_0} \tag{9}$$

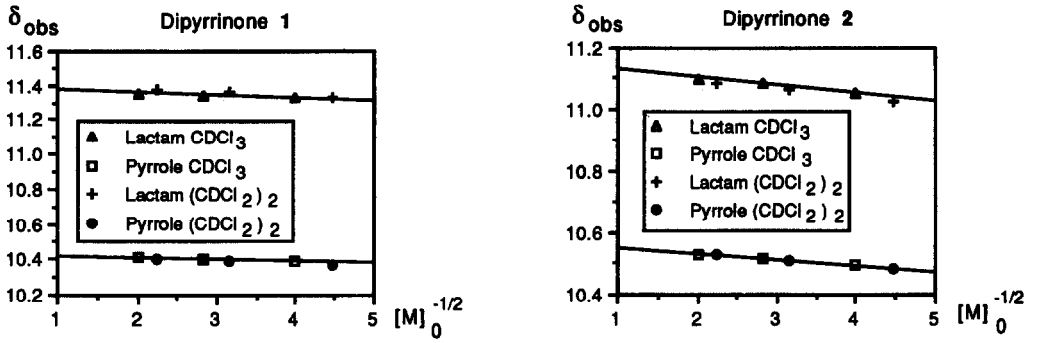

FIGURE 6. Plots of pyrrole and lactam N-*H* δ_{obs} *vs* $[M]_0^{-1/2}$ for extrapolating δ_{obs} to δ_D at large values of $[M]_0$ (Table 1, Figure 5) for the pyrrole N-*H* of dipyrrinones **1** and **2** in $CDCl_3$ and $(CDCl_2)_2$ solvent at 22°C. In the limit $[M]_0^{-1/2} \rightarrow 0$, $\delta_{obs} \rightarrow \delta_D$.

Extrapolation to δ_D can be accomplished at the lowest reasonable temperature and in the limit of high $[M]_0$, i.e., when $8\ K_A\ [M]_0 \gg 1$. Then the expression $\{(1 + 8\ K_A\ [M]_0)^{1/2} - 1\}$ approaches $(8\ K_A\ [M]_0)^{1/2}$, and equation (9) may be rewritten as:

$$\delta_{obs} \approx \delta_D - (\delta_D - \delta_M)\ (2\ K_A)^{-1/2}\ [M]_0^{-1/2} \qquad (10)$$

A plot (Figure 6) of the experimental pyrrole N-*H* δ_{obs} *vs* $[M]_0^{-1/2}$ in $CDCl_3$ or $(CDCl_2)_2$ at 22°C for the largest values of $[M]_0$ (Table 1), where the curves of Figure 5 start to flatten out, are found by a least squares procedure to fit the line $\delta_{obs}=10.430 - 0.00996\ [M]_0^{-1/2}$ for **1**, and $\delta_{obs}=10.569 - 0.0186\ [M]_0^{-1/2}$ for **2**. Within the constraints $\delta_D - \delta_M = 0.00996\ (2K_A)^{1/2}$ for **1** and $\delta_D - \delta_M = 0.0186\ (2K_A)^{1/2}$ for **2**, the extrapolated pyrrole N-*H* chemical shift of the pure dimer is thus $\delta_D=10.430$ for **1** and $\delta_D=10.569$ for **2**. Similarly, plots of the lactam N-*H* δ_{obs} *vs* $[M]_0^{-1/2}$ (Figure 5) in the limit of highest $[M]_0$ gives straight lines: $\delta=11.387 - 0.0150\ [M]_0^{-1/2}$ for **1** and $\delta_{obs}=11.151 - 0.0252\ [M]_0^{-1/2}$ for **2**. Thus the extrapolated lactam δ_D for the pure dimer is $\delta_D=11.387$ for **1** and $\delta_D=11.151$ for **2**.

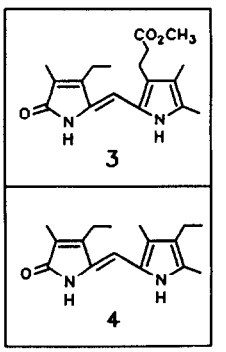

The pyrrole and lactam N-*H* δ_D values for **1** may be compared with those extrapolated for two dipyrrinones closely related to **1**, methyl ψ-xanthobilirubinate (**3**) and kryptopyrromethenone (**4**). Using the same extrapolation method, δ_D pyrrole N-*H* is found to be 10.425 for **3** and 10.437 for **4**. The pyrrole and lactam N-*H* values of **3** and **4** are quite close to those of **1**, and similar to those of **2**.

Extrapolation to δ_M can be accomplished in the limit of high dilution and/or high temperature. Plots of δ_{obs} *vs* $[M]_0$ (Figure 5) show a very steep convergence of δ_{obs} toward δ_M as $[M]_0$ approaches zero. A plot of log $[M]_0$ *vs* δ_{obs} should provide the needed scale expansion in the critical region of high dilution. The shape of such plots and the difficulties inherent in extrapolating δ_{obs} to δ_M in the region of high dilution is revealed in a series of theoretical curves (Figure 7) relating a computed δ_{obs} to log $[M]_0$ for different sets of δ_M and K_A values and a fixed δ_D ($\delta_D=10.430$ for N-*H* of **1**). The plots of Figure 7 reveal the sensitivity of δ_M to K_A and, in particular, the difficulty of extrapolating δ_{obs} to δ_M when K_A is large. Thus, for larger

K_A values the plots are steeper, and one must go to higher dilution to reach the foot of the curve where δ_{obs} *vs* $[M]_0$ approaches a horizontal line and where $\delta_{obs} \rightarrow \delta_M$.

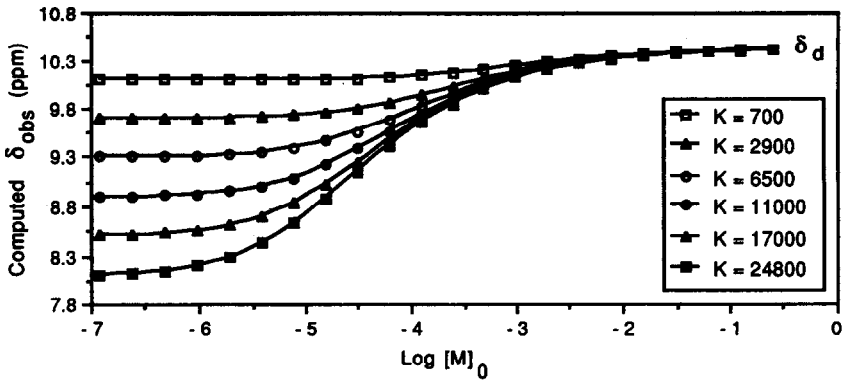

FIGURE 7. Theoretical plots of computed δ_{obs} *vs* log $[M]_0$ at 22°C for a given value of δ_D (10.430 ppm, pyrrole N-*H* of **1**). The computed values of δ_{obs} come from solving equation (8) for each value of $[M]_0$ (*e.g.* Table 1).

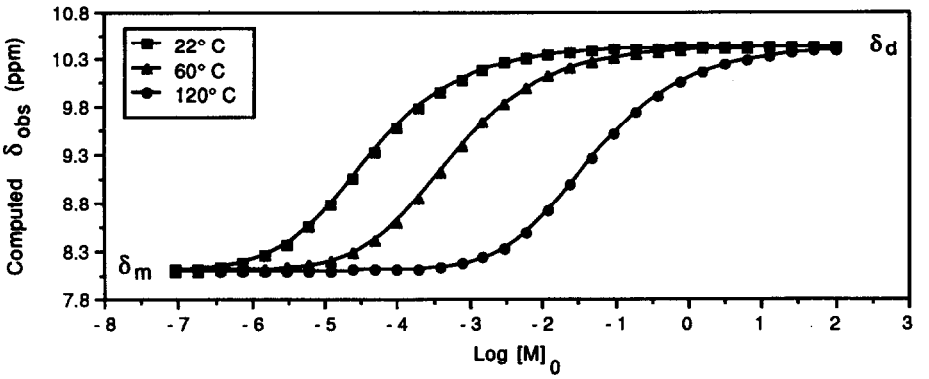

FIGURE 8. Theoretical plots of computed δ_{obs} *vs* log $[M]_0$ for fixed δ_M (8.1 ppm) and δ_D (10.430 ppm) at 22°, 60° and 120 °C, where K_A takes on values 24,800, 1,500 and 20 M^{-1}, respectively.

The behavior of the curves of Figure 7 with changing K_A also suggests that at higher temperatures, where K_A becomes reduced, extrapolating of δ_{obs} to δ_M should become easier. Support for this notion may be found in the curves of Figure 8 which relate computed δ_{obs} *vs* log $[M]_0$ for K_A at 22°, 60° and 120°C for constant δ_D (10.430 ppm) and δ_M (8.1).[12] The plots show that a curve taken from Figure 7 (—■—, K_A= 24,800, δ_M= 8.1) at 22° starts its ascent at much lower monomer concentration than curves at higher temperatures. Thus, the higher temperature curves have a longer and flatter foot at low [M]. As expected, $\delta_{obs} \rightarrow \delta_M$ at higher $[M]_0$, and thus it is clearly easier to determine δ_M (extrapolate δ_{obs} to δ_M) in the limit $[M]_0 \rightarrow 0$ at high temperatures (where K_A is smaller).

Unfortunately, the relatively low boiling point of $CDCl_3$ (~61°C) thwarted our attempts to find δ_M by lowering K_A. So we turned to a higher boiling (bp 147°C) solvent, $(CDCl_2)_2$, with solvation properties much like $CDCl_3$ for measurements at higher temperatures, up to 120°C. It may be noted that plots of experimental δ_{obs} *vs* $[M]_0$ for **1** and **2** (Figures 5 and 6) at 22°C in these two solvents are identical. And as shown in

Figure 9, plots of experimental δ_{obs} *vs* log $[M]_0$ for 1 in $CDCl_3$ and $(CDCl_2)_2$ are identical, within experimental error, over the measurable range of $[M]_0$ at 60°C (see Table 2). Consequently, we feel comfortable using δ_M, δ_D data from $(CDCl_2)_2$ and $CDCl_3$ interchangeably. The plots of Figure 9 clearly indicate the temperature effect on the monomer $\rightleftarrows$ dimer equilibrium of 1: for a given $[M]_0$, [M] increases as the temperature

TABLE 2. Similarity of Pyrrole and Lactam N-*H* Chemical Shifts (δ_{obs}) in (a) $(CDCl_2)_2$ and (b) $CDCl_3$ Solvents.

Dipyrrinone 1 Concentration (*M*)	Pyrrole Chemical shift (ppm) at			Lactam Chemical shift (ppm) at		
	60°C (a)	120°C (a)	60°C (b)	60°C (a)	120°C (a)	60°C (b)
0.000786076	9.588	8.395		10.103	8.218	
0.000778797			9.677			10.222
0.000623101	9.523	8.292		10.035	8.073	
0.000541266	9.480	8.230		9.962	8.230	
0.000393038	9.362	8.130		9.736	7.803	
0.000389399			9.450			9.866
0.000311551	9.266	8.096		9.644	7.764	
0.000270633	9.225	8.103		9.546	7.762	
0.000196519	9.094			9.300		
0.000194699			9.155			9.410
0.000155775	8.960			9.164		
0.000135317	8.961			9.092		
0.00009735			8.863			
0.000077888	8.729			8.810		
0.000067659	8.624			8.624		
Dipyrrinone 2 Concentration	Pyrrole Chemical shift (ppm) at			Lactam Chemical shift (ppm) at		
	60°C (a)	120°C (a)	60°C (b)	60°C (a)	120°C (a)	60°C (b)
0.022516		9.434			9.434	
0.011258		9.108			9.108	
0.005629		8.831			8.731	
0.0028145		8.590			8.462	
0.00140725		8.318			8.380	
0.001124834			9.477			9.477
0.000976563						
0.000706954	9.050	8.137		8.838	7.417	
0.000562417			9.175			9.039
0.000538079	8.878	8.065		8.567	7.312	
0.000488282						
0.000353477	8.720	7.974		8.321	7.162	
0.000281209			8.851			8.539
0.00026904	8.565	7.937		8.077	7.112	
0.000244141						
0.000176738	8.399	7.862		7.826		
0.000140604			8.547			8.046
0.00013452	8.274			7.634		
0.000122071						
0.000088369	8.151			7.442		

increases and hence δ_{obs} decreases and approaches a limiting value (δ_M). At 120°C the experimental points begin to approach, then fall on, a horizontal line near δ=8.1. Figure 9 also illustrates the difficulty in extrapolating δ_{obs} to δ_M at lower temperatures where the equilibrium favors dimer. At 22°C the measureable δ_{obs} at the limit of instrument (500 MHz NMR) sensitivity is still far from δ_M and hence far from the flat region of the curve where δ_M can be extrapolated most reliably.

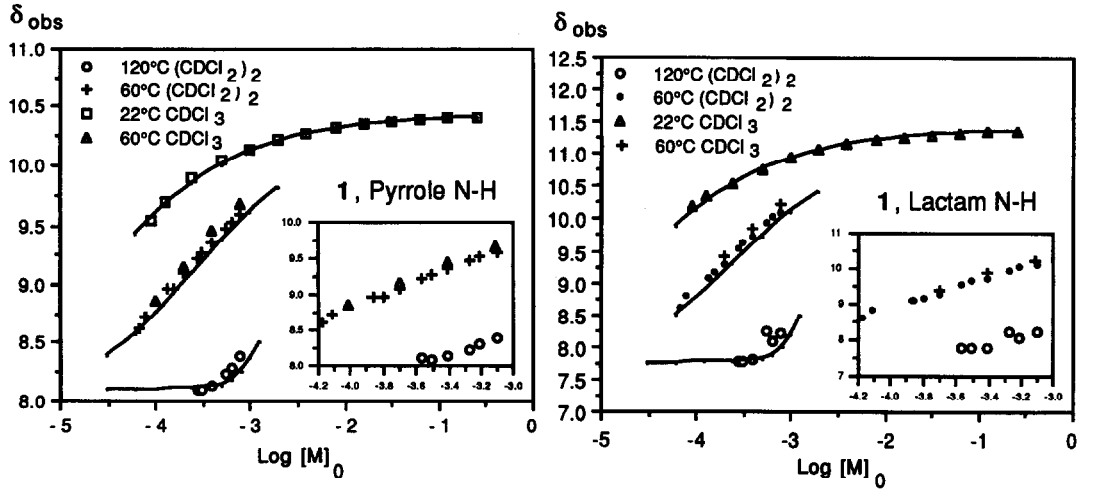

FIGURE 9. Experimental points (δ_{obs} *vs* $[M]_0$) for the pyrrole (left) and lactam (right) N-*H* of **1** at 22° and 60°C in $CDCl_3$ and at 60° and 120°C in $(CDCl_2)_2$. The lines are the computed curves for δ_{obs} *vs* $[M]_0$ when δ_M = 8.1, δ_D 10.43 and is 24,800 at 22°, 1,500 at 60° and 20 at 120°C. The inset is an expansion of the δ_{obs} *vs* $[M]_0$ plot at low sample concentration. At 22°C, the two points below log $[M]_0 \simeq$ -3.6 were determined at 500 MHz and represent the sensitivity limits for the instrument for detecting the pyrrole N-*H* of **1**.

Reassuringly, the experimental points of Figure 9 fall on the theoretical curves relating computed δ_{obs} to log $[M]_0$ for δ_M= 8.1, δ_D=10.430 and K_A values for 22°, 60° and 120°C. Plots and curves similar to those of Figure 9 are found for the lactam N-*H* of **1** (Figure 9) and for the pyrrole and lactam N-H's of **2**. Again, since **1** and **2** have large K_A values at 22°C and the dilution required for $\delta_{obs} \rightarrow \delta_M$ is outside the range of even the highest field NMR instruments, we plot experimental δ_{obs} *vs* log $[M]_0$ at 120°C in $(CDCl_2)_2$ solvent in order to extrapolate δ_{obs} to δ_M. The extrapolated δ_M values for the pyrrole N-*H* chemical shifts of **1** and **2** are 8.10 and 7.75 ppm, respectively. And the extrapolated δ_M values for the lactam N-*H* chemical shifts of **1** and **2** are 7.75 and 7.00 ppm, respectively.

Extrapolation to K_A can be achieved from the variation of δ_{obs} with $[M]_0$ expressed in equation (6). Thus, using the experimental data of Table 1 and the extrapolated values for δ_D and δ_M, plots of the right side of equation (6), *viz.* $\{\log(\delta_{obs}-\delta_M) - 2\log(\delta_D-\delta_{obs})\}$ *vs* log $[M]_0$ gives straight lines (Figure 10) with slope=1 and intercepts equal to $\{\log 2/(\delta_D-\delta_M) + \log K_A\}$. From the intercept, K_A at 22°C may be calculated for **1** and **2**. The discrepancy between the K_A values derived from δ_{obs} for the pyrrole and lactam N-*H* (Table 1) is probably related to a greater inaccuracy in determining δ_{obs} for the broader lactam N-*H* resonance. We estimate (based on reproducibility) that our K_A values are only good to $\pm$10%, and the values derived from δ_{obs} for lactam N-*H* resonances at 22°C may have a greater error; however, some measurements gave results within 3-4% of each other.

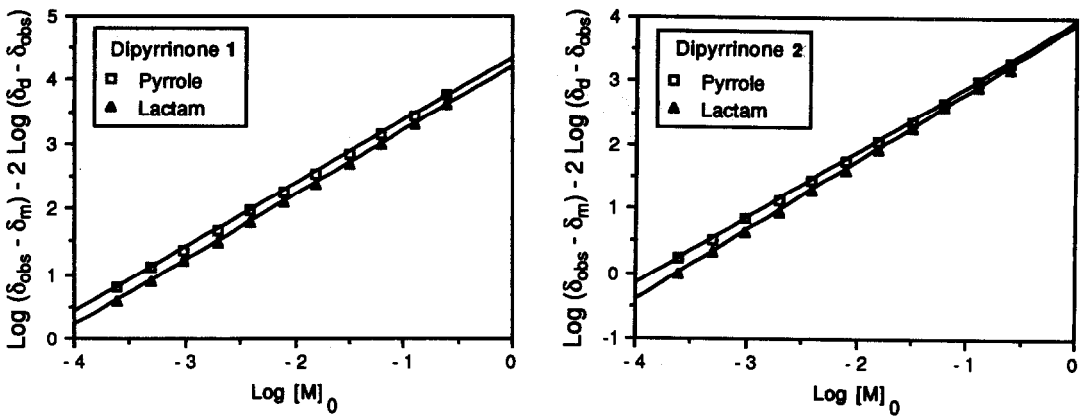

FIGURE 10. Plots of $\log(\delta_{obs} - \delta_M) - 2\log(\delta_D - \delta_{obs})$ *vs* $\log [M]_0$ for the pyrrole and lactam N-*H* signals of dipyrrinones 1 and 2 in $CDCl_3$ solvent at 22°C. The values of δ_D and δ_M are from Figures 5 and 8, respectively; δ_{obs} and $[M]_0$ are from Table 1. The best fit lines for the pyrrole N-*Hs* have intercepts = 4.327 and 3.919 for 1 and 2, respectively; hence K_A = 24,800 M^{-1} for 1 and 11,700 M^{-1} for 2. The best fit lines for the lactam N-*Hs* have intercepts 4.193 and 3.879 for 1 and 2, respectively; hence K_A = 28,600 M^{-1} for 1 and 15,700 M^{-1} for 2.

Similar plots for δ_{obs} *vs* $[M]_0$ determined at 37° and 52° gave straight line plots similar to those of Figure 10 when the same extrapolated δ_M and δ_D values[12] were used in equation (6). These are summarized in Table 3 along with thermodynamic parameters for the monomer ⇄ dimer association equilibrium determined in the usual way. It is satisfying to note that the extrapolated K_A for 1 at 37°C corresponds reasonably well to value (1700 M^{-1}) determined by vapor phase osmometry in $CHCl_3$.[3,10] Interestingly, the K_A for 2 is smaller than that of 1 by a factor of ~40%. The C(9) CH_3 of 1 apparently exerts no non-bonded steric destabilization in the dimer and even appears to exert a greater stabilizing influence than a hydrogen at C(9). The reasons for this are unclear; however, molecular dynamics calculations (SYBYL; Evans & Sutherland ESV-10$^+$ workstation) on the relative stability of the dimer *vs* two monomers indicates that the dimer of 1 is relatively more stable (2 kcal/mole) than that of 2 — in good agreement with the differences in experimental ΔH°_{eq} values for 1 and 2.

TABLE 3. Summary of K_A Values for the Monomer ⇄ Dimer Equilibrium of Dipyrrinones 1 and 2 in $CDCl_3$ or $(CDCl_2)_2$ at 22°, 37° and 52°C as Determined from Extrapolated Pyrrole and Lactam N-*H* Chemical Shifts for Pure Monomer (δ_M) and Dimer (δ_D). Thermodynamic Parameters for the Equilibrium (ΔG°_{eq}, ΔH°_{eq}, ΔS°_{eq}) are Determined from the Temperature Dependence of K_A.

Parameter Determined for/from:	Methyl Xanthobilirubinate (1)		Methyl Neoxanthobilirubinate (2)	
	Pyrrole N-*H*	Lactam N-*H*	Pyrrole N-*H*	Lactam N-*H*
δ_D (ppm)	10.43	11.39	10.57	11.15
δ_M (ppm)	8.10	7.75	7.75	7.10
K_A (M^{-1}) at 22°C	24,800	28,600	11,700	15,700
K_A (M^{-1}) at 37°C	4,900	5,100	3,200	3,600
K_A (M^{-1}) at 52°C	1,800	1,800	1,300	1,200
ΔH°_{eq} (kcal/mole)	-16.85	-17.58	-14.13	-16.39
ΔS°_{eq} (cal/°/mole)	-37.2	-39.4	-29.4	-36.5

SUMMARY

Self-association of dipyrrinones can be detected by ^{1}H-NMR NOE. The dimerization association constant (K_A) can be determined from an analysis of NMR chemical shifts of the pyrrole and lactam N-*H*. First, N-*H* chemical shift values for the pure dimer (δ_D) and pure monomer (δ_M) are obtained by extrapolation methods. Then, these parameters and experimentally-determined N-H chemical shifts (δ_{obs}) for a range of dipyrrinone concentrations ($[M]_0$) are plotted in equation (6) to extrapolate K_As. The extrapolated data for the dipyrrinones of this study are summarized in Table 4.

TABLE 4. Extrapolated values of δ_D, δ_M and K_A for Dipyrrinones **1-4** in $CDCl_3$ at 22°C.

Dipyr-rinone	δ_D (Dimer) ppm		δ_M (Monomer) ppm		K_A (M^{-1}) Determined from	
	Pyrrole N-*H*	Lactam N-*H*	Pyrrole N-*H*	Lactam N-*H*	Pyrrole N-*H*	Lactam N-*H*
1	10.43	11.39	8.10	7.75	24,800	28,600
2	10.56	11.15	7.75	7.00	11,700	15,700
3	10.43	11.40	8.10[a]	7.75[a]	23,000	24,000
4	10.44	11.42	8.10[a]	7.75[a]	23,000	22,000

[a] Assumed from the data for **1**.

EXPERIMENTAL PART

All NMR spectra were run on a GE QE-300 FT spectrometer in either deuteriochloroform (99.9% d_1) or dimethylsulfoxide-d_6 (99.9% d_6), both from Aldrich. Infrared spectra were run on a Perkin-Elmer 1610 FT-IR spectrophotometer. All UV-visible absorption spectra were run on a Perkin-Elmer model 3840 diode array instrument. Analytical thin layer chromatography (tlc) was carried out on J.T. Baker silica gel 1B-F plates (125 μ layer). Column chromatography was carried out on 32-63 μ activated silica gel for medium pressure chromatography (M. Woelm). High performance liquid chromatographic (HPLC) analyses used a detector set at 410 nm and a Beckman-Altex Ultrasphere-IP 5 μm C-18 ODS column (25 x 0.46 cm), with a Beckman ODS precolumn (4.5 x 0.46 cm) and a flow of 0.75 ml/minute of 0.1 *M* di-n-octylamine acetate in 5% aq. methanol as eluent. Pentane-2,4-dione, ethyl acetoacetate, ethyl acrylate, acetic acid, ethyl acetate, benzene, acetone and hexane were from Aldrich. Spectral grade methanol, chloroform, benzene and dimethylsulfoxide were from Fisher. Methanol (HPLC grade) was from Fisher.

Methyl Xanthobilirubinate (1) was prepared and purified as described previously,[13] in 72% yield. It had, m.p. 215-217°C (Lit.[13] mp 217-220°C)

UV-vis: λ_{max} 406, ϵ 34,000 ($CHCl_3$); λ_{max} 411, ϵ 37,700 (CH_3OH); λ_{max} 412, ϵ 34,400 (DMSO).

IR (film): ν = 3346, 3161, 2965, 1736, 1676, 1632, 1267, 1175 cm^{-1}.

^{1}H-NMR ($CDCl_3$/TMS) δ: 1.17 (t,3H,7.5 Hz), 1.94 (s,3H), 2.14 (s,3H), 2.41 (s,3H), 2.46 (t,2H, J= 7.2 Hz), 2.54 (q,2H,J=7.5 Hz), 2.74 (t,2H,J=7.2 Hz), 3.68 (s,3H), 6.13 (s,1H), 10.41 (s,1H), 11.36 (s,1H) ppm.

^{13}C-NMR ($CDCl_3$/TMS) δ: 8.53(q), 9.60(q), 11.57(q), 15.08(q), 17.96(t), 19.88(t), 35.13(t), 51.56(q), 101.04(d), 119.03(s), 122.40(s), 122.43(s), 124.57(s), 127.10(s), 131.65(s), 148.29(s), 173.59(s), 173.92(s).

Methyl Neoxanthobilirubinate (2) was prepared from **1** as follows.

Methyl xanthobilirubinate (**1**) was converted smoothly in one step to mesobiliverdin-XIIIα dimethyl ester[14] via and oxidative self-coupling reaction, as reported previously. Scission of the verdin was accomplished as described by Manitto[15] for biliverdin-IXα dimethyl ester. Thus, thiobarbituric acid (50 mg) was added to a stirred solution of mesobiliverdin-XIIIα dimethyl ester (140 mg, 0.23 mmol) dissolved in ethyl acetate (300 mL). The reaction was carried out in the dark at room temperature under nitrogen. After 6 hours, the solvent was removed (roto-vap) and the residue was redissolved in a minimal amount of hot chloroform. A volume of hexane (equal to 10 x the volume of chloroform) was added and a violet precipitate

was removed by filtration, leaving a yellow solution containing **2**. The solvent was then evaporated and the residue was taken up in a minimum volume of chloroform. The precipitation cycle was repeated three times.

m.p. 170-172°C (Lit.[16] mp 174°C)

UV-vis: λ_{max} 388 nm, ϵ 29,000 ($CHCl_3$); λ_{max} 395 nm, ϵ 27,500 (CH_3OH); λ_{max} 390 nm, ϵ 31,000 (DMSO).

IR (KBr) ν: 3366, 3147, 2973, 1227, 1654, 1619, 1278, 1256, 1170, 984, 812, 706 cm.

^{1}H-NMR ($CDCl_3$/TMS) δ: 1.160 (t,3H,J=7.5 Hz), 1.927 (s,3H), 2.124 (s,3H), 2.555 (q,2H,J=7.5 Hz), 2.565 (t,2H,J=7.2 Hz), 2.763 (t,2H,J=7.2 Hz), 3.667 (s,3H), 6.120 (s,1H), 6.806 (d,1H,J=1.5 Hz) 10.285 (bs,1H), 10.733 (bs,1H) ppm.

^{13}C-NMR ($CDCl_3$/TMS) δ: 8.09(q), 9.40(q), 14.91(q), 17.98(t), 20.76(t), 34.88(t), 51.56(q), 101.06(d), 120.65(d), 122.70(s), 123.44(s), 123.45(s), 124.46(s), 128.62(s), 148.49(s), 173.71(s), 174.33(s) ppm.

Acknowledgement. We thank the National Institutes of Health (HD 17779) for generous support of this work and Professor John H. Frederick and Mr. Blake R. Peterson, as well as Mr. Zhang Xien-Fu and Prof. Xu Hui-Jin (Institute of Photographic Chemistry) for assistance with the computational method.

REFERENCES AND NOTES

1. Lightner, D.A.; McDonagh, A.F. *Accounts Chem. Res.* **1984**, *17*, 417-424.
2. McDonagh, A.F.; Lightner, D.A. *Pediatrics* **1985**, *75*, 443-455.
3. For leading references, see H. Falk, *The Chemistry of Linear Oligopyrroles and Bile Pigments*, Springer-Verlag, N.Y. **1989**, p 142.
4. Trull, F.R.; Ma, J.S.; Landen,G.L.; Lightner, D.A. *Isr. J. Chem.* **1983**, *23*, 211-218.
5. (a) Kaplan, D.; Navon, G. *Isr. J. Chem.* **1983**, *23*, 177-186.
   (b) Kaplan, D.; Navon, G. *Biochem. J.* **1982**, *201*, 605-613.
   (c) Navon, G.; Frank, S.; Kaplan, D. *J. Chem. Soc. Perkin Trans 2*, **1984**, 1145-1149.
6. (a) Zhang, M.H.; Lightner, D.A. *Tetrahedron Lett.* **1987**, *27*, 4033-4036.
   (b) Lightner, D.A.; Person, R.V.; Peterson, B.R.; Puzicha, G.; Pu, Y-M.; Bojadziev, S. *Biomolecular Spectroscopy II* (Birge, R.R.; Nafie, L.A., eds.), Proc. SPIE *1432*, **1991**, 2-13.
7. Lightner, D.A.; Reisinger, M.; Wijekoon, W.M.D. *J. Org. Chem.* **1987**, *52*, 5391-5395.
8. Lightner, D.A.; Ma, J.S.; Adams, T.C.; Franklin, R.W.; Landen, G.L. *J. Heterocyclic Chem.* **1984**, *21*, 139-144.
9. Cullen, D.L.; Black, P.S.; Meyer, E.F.; Lightner, D.A.; Quistad, G.B.; Pak, C-S. *Tetrahedron* **1977**, *33*, 477-483.
10. (a) Falk, H.; Grubmayr, K.; Hollbacher, O.; Leodolter, A.; Neufingerl, F.; Ribó, J.M. *Monatsh. Chem.* **1977**, *108* 1113-1130.
    (b) Falk, H.; Schlederer, T.; Wolschann, P. *Monatsh. Chem.* **1981**, *112*, 199-207.
11. The lactam N-*H* chemical shifts are broader and weaker than those of the pyrrole and are therefore less useful for extrapolation of δ_M at low sample concentration.
12. For a given solvent, δ_D and δ_M are believed to be intrinsic, temperature-independent properties of a compound.
13. Shrout, D.P.; Lightner, D.A. *Synthesis*, **1990**, 1062-1065.
14. Trull, F.R.; Franklin, R.W.; Lightner, D.A. *J. Heterocyclic Chem.* **1987**, *24*, 1573-1579.
15. Manitto, P.; Monti, D. *J.C.S. Chem. Comm.*, **1980**, 178-180.
16. Fischer, H.; Orth, H. *Die Chemie des Pyrrols*, Vol. II first half, Akademische Velagsgesellschaft, m.b.h., Leipzig **1937**, p 135.